A New Approach to Detect Ground Clutter Mixed With Weather Signals

Yinguang Li, Guifu Zhang, *Senior Member, IEEE*, Richard J. Doviak, *Life Fellow, IEEE*, Lei Lei, and Qing Cao, *Member, IEEE*

***Abstract*—Considering that the statistics of the phase and the power of weather signals in the spectral domain are different from those statistics for echoes from stationary objects, a spectrum clutter identification (SCI) algorithm has been developed to detect ground clutter using single polarization radars, but SCI can be extended for dual-pol radars. SCI examines both the power and phase in the spectral domain and uses a simple Bayesian classifier to combine four discriminants: spectral power distribution, spectral phase fluctuations, spatial texture of echo power, and spatial texture of spectrum width to make decisions as to the presence of clutter that can corrupt meteorological measurements. This work is focused on detecting ground clutter mixed with weather signals, even if the clutter power to signal power ratio is low. The performance of the SCI algorithm is shown by applying it to radar data collected by University of Oklahoma-Polarimetric Radar for Innovation in Meteorology and Engineering.**

***Index Terms*—Bayesian methods, meteorological radar, radar clutter, radar detection, spectral analysis.**

I. Introduction

GROUND clutter is received when the mainlobe or sidelobes of the antenna illuminate objects on the ground. Weather data can be highly contaminated by ground clutter if the radar is measuring precipitation near the ground using elevation angles θ_e less than a beamwidth. Data at low θ_e is required to have accurate estimates of rainfall for long ranges. However, clutter power can strongly bias the estimated spectral moments of the weather signal. The estimated reflectivity of the weather signal will be biased high, and the estimated mean radial velocity of the weather signal will be biased toward zero, but the estimated spectrum width bias has a more complicated dependence on the clutter to signal power ratio (CSR), mean radial velocity, and spectrum width of the weather signal.

Resolution volumes having weather signals contaminated by ground clutter can be identified using a pre-stored static clutter map (i.e., the static clutter map or bypass map is determined from a series of radar images in clear-air conditions, Meischner [1]). The main disadvantage of using static clutter map is that it cannot find clutter locations that appear only under anomalous propagation (AP) conditions. Lee *et al.* [2] introduced a decision tree algorithm, and it was implemented at the three radar sites of Meteo-Swiss Monte Lema, La Dole, and Albis. The algorithm made a clutter/nonclutter decision using the radial velocity, the spectrum width, the minimum detectable signal, the one-lag and two-lag signal fluctuations, the vertical gradient of reflectivity, and a continuously updated clutter map. Kessinger *et al.* [3] introduced a radar echo classifier (REC) which was deployed by National Weather Service's WSR-88D in 2003, and it uses fuzzy logic to classify the type of radar echoes. The REC algorithm includes detection of AP, precipitation, insects, and sea clutter. The clutter mitigation decision (CMD) algorithm was introduced by Hubbert *et al.* [4], [5] and evaluated by Ice *et al.* [6]. Hubbert *et al.* give a detailed discussion of ground clutter detection algorithms. Among the long standing problems in clutter detection and/or filtering, are 1) false detections along zero isodops and 2) missed detections for multiple clutter sources [7]. Another clutter detection algorithm, but combined with a ground clutter filter, is the clutter environment analysis using adaptive processing (CLEAN-AP) which was recently introduced by Warde and Torres [8]. This algorithm takes advantage of the phase of the coefficients in the auto-correlation spectral density. It is stated in [7] that CLEAN-AP has better ground-clutter mitigation (detection and filtering) than the current CMD/Gaussian model adaptive processing (GMAP) [9]. Zhang *et al.* [10] introduced a multipattern technique to mitigate clutter received via sidelobes using a phased array radar (i.e., the National Weather Radar Testbed in Norman, OK). The multipattern technique not only mitigates ground clutter but also moving clutter that cannot be removed by conventional ground clutter detection algorithms.

In addition to the clutter detection algorithms based on single polarization radar data, researchers have also introduced clutter detection algorithms based on dual polarization radar data [11]–[14]. In this paper, the spectrum clutter identification (SCI) algorithm is developed for the single polarization radars, which are still widely used in many places.

Manuscript received July 4, 2012; accepted July 15, 2012. Date of publication August 31, 2012; date of current version March 21, 2013. This work was supported in part by the National Oceanic and Atmospheric Administration's National Severe Storms Laboratory under the cooperative Agreement NA08OAR4320904 and the National Science Foundation under Grant of AGS-1046171.

Y. Li and L. Lei are with the School of Electrical and Computer Engineering, University of Oklahoma, Norman, OK 73019-1102 USA, and also with Advanced Radar Research Center, University of Oklahoma, Norman, OK 73072-7307 USA (e-mail: yinguangli@ou.edu; leilei@ou.edu).

G. Zhang is with the School of Meteorology, University of Oklahoma, Norman, OK 73072-7307 USA, and also with Advanced Radar Research Center, University of Oklahoma, Norman, OK 73072-7307 USA (e-mail: guzhang1@ou.edu).

R. J. Doviak is with the National Severe Storm Laboratory, Norman, OK 73072 USA.

Q. Cao is with Advanced Radar Research Center, University of Oklahoma, Norman, OK 73072-7307 USA (e-mail: qingcao@ou.edu).

Color versions of one or more of the figures in this paper are available online at http://ieeexplore.ieee.org.

Digital Object Identifier 10.1109/TGRS.2012.2209658

TABLE I
QUALITATIVE EXPECTED VALUES OF SPD GIVEN DIFFERENT SPECTRA

	Clutter only (Fig.1a)	Weather only $\lvert v_{rw}\rvert \le 1$ m s^{-1} (Fig.1b)	Weather only $\lvert v_{rw}\rvert > 1$ m s^{-1}	Weather & clutter (not overlapped) (Figs. 1c,d)	Weather & clutter (overlapped) (Figs. 1e, f)
SPD	Large	$g(\sigma_{vw})$	Small	h(CSR)	u(CSR,v_{rw}, σ_{vw}.)

Ground clutter detection methods locate regions where spectral moments are significantly biased by ground clutter, so ground clutter filters (e.g., GMAP [9] or a regression filter [15]) can be applied. This avoids application of the filter in locations where pure weather signals are located, but clutter is not present.

A simple Bayesian classifier (SBC) is used to make decisions as to the presence of ground clutter. It is based on applying Bayes' theorem with strong independence assumptions. In spite of its naïve design and over-simplified assumptions, SBC has worked quite well in many complex real-world situations [16]–[18]. Based on [19], it is stated that SBC can be optimal under zero-one loss (misclassification loss) even when the assumption class-conditional independence is violated by a wide margin.

In Section II, the SCI algorithm is developed. SCI combines the information provided by four discriminants: the spectral power distribution (SPD), spectral phase fluctuations (SPF), the spatial texture of echo power [i.e., power texture (PT)], and the spatial texture of spectrum width [i.e., spectrum width texture (SWT)]. This section focuses on detecting ground clutter mixed with weather signals, even if the CSR is low but can still significantly bias spectral moment estimates. In Section III, the SCI algorithm is applied to data collected by the University of Oklahoma-Polarimetric Radar for Innovation in Meteorology and Engineering (OU-PRIME). A summary and discussions are presented in the last section.

II. SCI ALGORITHM

The weather signal voltage is $V(t) = I(t) + jQ(t)$, and its Fourier transform is $X(v) = A(v)e^{j\xi(v)}$ where $A(v)$ is the amplitude and $\xi(v)$ is the phase of the spectral coefficient at the apparent Doppler velocity v [20]; herein, v will simply be called the Doppler velocity. First, let us start with the clutter discriminant based on the spectral power.

A. SPD

In this section, SPD is defined, and examples of its properties are shown when it is applied to combined simulated clutter and weather signal spectra of various CSRs. The SPD is calculated using the power spectrum $P(v)$ [i.e., $A^2(v)$]. The SPD is an indicator of how much power exists in the interval $2\sqrt{2}\Delta v_w$ centered on zero Doppler velocity and how significant this power is as compared to power outside the interval. SPD is defined as

$$\text{SPD} = \frac{\sum_{-\sqrt{2}\Delta v_w}^{+\sqrt{2}\Delta v_w} P(v)}{\sum_{-v_N}^{+v_N} P(v) - \sum_{-\sqrt{2}\Delta v_w}^{+\sqrt{2}\Delta v_w} P(v)}. \tag{1}$$

In (1)v_N is the Nyquist velocity; $(\Delta v_w)^2$ is the second central moment of the observed clutter power spectrum. $(\Delta v_w)^2$ is principally due to the window function (Section II-A1), and $\pm\sqrt{2}\Delta v_w$ is the interval wherein the spectral power and phase characteristics of clutter and weather are examined. The larger is SPD, the more is power located within $\pm\sqrt{2}\Delta v_w$ relative to the power outside this interval; therefore, SPD is related to CSR. SPD is similar to clutter ratio narrow (CRN) introduced by [5]. CRN is the ratio of power within ± 0.5 m s^{-1} to that outside ± 0.5 m s^{-1} but within ± 2 m s^{-1}. Thus, CRN examines the power distribution around zero velocity whereas SPD examines the distribution for the entire spectrum. The CRN is not used in CMD because, as stated in [5], clutter phase alignment (CPA), a discriminant used in CMD, better discriminates narrow weather and clutter spectra than does CRN.

In Table I, the qualitative expected values of SPD given different conditions of weather signals and clutter are summarized, and functions g, h, and u indicate SPD is a function of the specified arguments.

A numerical simulation [21]–[23] is used to obtain some representative simulated power spectra of clutter mixed with weather signals shown in Fig. 1. The parameters of the simulation are in Table II; these match those of OU-PRIME, the weather radar used to collect data used herein. In the simulation, the weather signal and clutter are the same in each of the panels; only the relative strength and the Doppler velocity of weather change. A Blackman window is applied to the simulated time-series data. The red portions of the curves in Fig. 1 are within $\pm\sqrt{2}\Delta v_w$. The CNR [Fig. 1(a)] or SNR [Fig. 1(b)] or signal plus clutter to noise ratio (SCNR) (i.e., $(S+C)/N$) [Fig. 1(c)–(f)] are all set to 60 dB. The CSR is equal to 20 dB in Fig. 1(c) and (e), and equal to -15 dB in Fig. 1(d) and (f). In the figure caption, v_{rc}, σ_{vc}, and σ_{vw} are the mean radial velocity and spectrum width of clutter and spectrum width of weather signals; the panel entry v_{rw} is the estimated mean radial velocity for the weather signals; likewise v_{rs} and σ_{vs} entries are estimates for the summed spectrum. The root mean square value of turbulent velocities is fixed at 1 m s^{-1}, and the mean power, mean radial

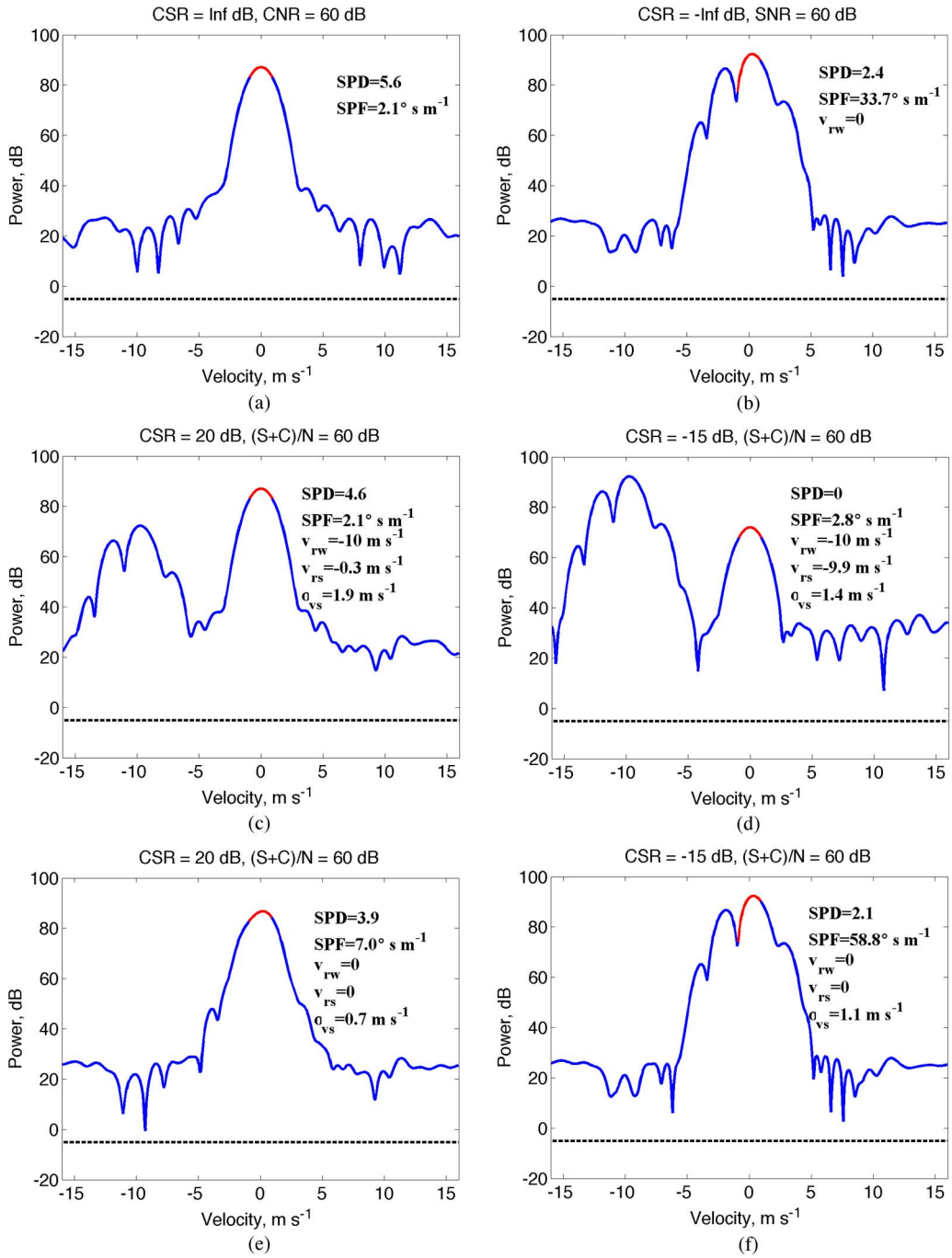

Fig. 1. Spectra of simulated clutter mixed with a simulated narrow-band weather signal. The black dashed line is the noise floor, and the red portions of the curves are within $\pm\sqrt{2}\Delta v_{\rm w}$. $v_{\rm rc}=0$, $\sigma_{\rm vc}=0.6$ m s^{-1} and $\sigma_{\rm vw}=1.0$ m s^{-1}.

velocity, and spectrum width are calculated in the spectral domain using all the spectral coefficients (i.e., no thresholds are applied). The spectral interval Δv between adjacent bins is equal to 0.1 m s^{-1}. The discriminant SPF is discussed in Section II-B.

In Fig. 1(a) and (b) (pure clutter and pure narrow-band weather signal), the SPD is equal to 5.6 and 2.4, respectively. The large difference between the two SPD values is caused by the fact that the clutter spectrum is still significantly narrower than the spectrum of the weather signal; thus significantly more clutter power is within the spectral interval $\pm\sqrt{2}\Delta v_{\rm w}$. The relatively large SPD difference suggests SPD has the capability to distinguish clutter from narrow-band zero-velocity weather signals.

In Fig. 1(c) and (d), the spectra of weather signal and clutter are not overlapped, and the SPD is equal to 4.6 and 0, respectively. SPD in panel (c) is larger than that in (d) because SPD (related to CSR) measures the ratio of power within $\pm\sqrt{2}\Delta v_{\rm w}$ (i.e., mostly clutter power) and those outside of it (i.e., mostly weather power). Fig. 1(c) shows the estimates of radial velocity $(v_{\rm rs}=-0.3)$ and spectrum width $(\sigma_{\rm vs}=1.9)$ of the summed spectra are significantly different from the weather signal's radial velocity $(v_{\rm rw}=-10)$ and spectrum width $(\sigma_{\rm vw}=1)$. Fig. 1(d) suggests insignificant velocity estimate error due to

TABLE II
RADAR AND METEOROLOGICAL PARAMETERS USED IN THE SIMULATION

wavelength (λ)	5.44 cm
One-way 3dB Beamwidth (θ_1)	0.5°
Scan Rate (α)	16° s^{-1} (0.28 radians per second)
Pulse Repetition Frequency (PRF)	1180 Hz
Number of Samples (M)	38
SCNR [(S+C)/N)]	60 dB
Turbulence Intensity (σ_t)	1 m s^{-1}
Mean Wind Velocity	0
Number of Stationary Scatterers	1
Number of Moving Scatterers	1000

TABLE III
MINIMUM CSR (dB), AS A FUNCTION OF WEATHER SIGNAL SPECTRUM WIDTH (σ_{vw}), THAT CAUSES BIASES OF 1 dB IN MEAN POWER (P_w) AND 1 m s^{-1} IN RADIAL VELOCITY (v_{rw}) AND σ_{vw} ESTIMATES OF WEATHER SIGNALS

	σ_{vw}=1	σ_{vw}=2	σ_{vw}=3	σ_{vw}=4	σ_{vw}=5	σ_{vw}=6
CSR(P_w)	-5.9	-5.9	-5.9	-5.9	-5.9	-5.9
CSR(v_{rw})	-11.8	-11.8	-11.8	-11.8	-11.8	-11.8
CSR(σ_{vw})	-19.2	-16.9	-15.3	-14	-12.8	-11.7

clutter (CSR $= -15$ dB), but spectrum width estimates with clutter (i.e., $\sigma_{vs} = 1.4$) are larger than $\sigma_{vw} = 1$, consistent with results to be shown in Table III.

According to NEXRAD Technical Requirements [24, Sec. 3.7.1.2.3.1], bias in the estimates of both mean radial velocity (v_{rw}) and spectrum width (σ_{vw}) of weather signals shall be no more than 1 m s^{-1}. The bias due to clutter assuming v_{rw} is at the Nyquist velocity (the worst case condition for σ_{vw} estimate bias) is numerically calculated for SNR = infinity, in which both clutter ($\sigma_{vc} = 0.6$ m s^{-1}) and weather ($\sigma_{vw} = 1$ m s^{-1}) spectra have Gaussian shape. The minimum CSRs that cause a 1 dB bias in mean power P_w and 1 m s^{-1} bias in v_{rw} and σ_{vw} estimates are shown in Table III.

If the mean radial velocity of weather signal (v_{rw}) is at the Nyquist velocity (i.e., 16.06 m s^{-1} for OU-PRIME), the CSR needs to be -5.9 dB to bias the mean power 1 dB, but it only needs to be -11.8 dB to bias v_{rw} by 1 m s^{-1}, independent of the spectrum width (σ_{vw}) of the weather signal. But if σ_{vw} equals 1 m s^{-1}, the CSR only needs to be -19.2 dB to bias σ_{vw} to 2 m s^{-1}. Thus, it is concluded detection of clutter down to a CSR $= -15$ dB is important considering the bias it can bring to the estimates of Doppler velocity and spectrum width; these two spectral moments place more stringent detection requirements on the clutter detectors than the error specified (i.e., 1 dB) for power measurements. If all the clutter power is within the interval $\pm\sqrt{2}\Delta v_w$ while all the weather power is outside of it, SPD $= 0.03$ if CSR $= -15$ dB.

In Fig. 1(e) and (f), the spectra of weather signal and clutter are overlapped, and the SPD is equal to 3.9 and 2.1, respectively. SPD in Fig. 1(e) is larger than that in Fig. 1(f) because the CSR is 20 dB and thus the SPD, as well as σ_{vs}, is more strongly influenced by clutter, whereas in Fig. 1(f) CSR is -15 dB and the weather spectrum mostly controls SPD. From Fig. 1(f), it can be seen that all the three radar moments of weather signals are almost equal to those of the summed spectra if the spectra are overlapped and CSR is equal to -15 dB or smaller.

1) Calculation of the Observed Clutter Spectrum Width: In this section, the spectral interval $\pm\sqrt{2}\Delta v_w$ is determined wherein the spectral power and phase characteristics of clutter and weather are examined to detect the presence of significant clutter. Δv_w is determined by the beam's scan rate, the *intrinsic* spectrum width of the clutter, the dwell time, and the window weighting function. In order to reduce overlapping of clutter and weather spectra caused by a rectangular window, a Blackman window with a maximum sidelobe level of 58.1 dB is applied to the time-series data [25].

The *observed (measured)* clutter spectrum is broader than the *intrinsic* spectrum of clutter. The *intrinsic* clutter spectrum (i.e., the spectrum associated only with the physical characteristics of clutter) is the spectrum observed with asymptotic data collection parameters (i.e., T_s, the pulse repetition time (PRT), goes to zero and T_d, the dwell time, goes to infinity) when the beam is not scanning. The *intrinsic* spectra of clutter

for urban, prairie, and wooded regions have been characterized, under conditions of full and light foliage and various intensities of wind, using a phased array radar and nearly asymptotic data collection parameters [26]. If the ground scatterers are fixed objects that do not move, nor have internal motions (henceforth these are called hard scatterers), the intrinsic clutter spectrum is a delta function centered on zero velocity.

The *asymptotic* clutter spectrum is the one observed with asymptotic data collection parameters when the beam is scanning. The asymptotic spectrum can, at best, only be approximated because an infinite dwell time would require spatial homogeneity (in a statistical sense) of the ground scatterers as they are being scanned. If the scatterers are many and hard, the *asymptotic* spectrum has a finite width proportional to the antenna diameter $D_{\rm a}$ and the angular scan rate α. The square of the asymptotic clutter spectrum width caused by a Gaussian-shaped beam pattern scanning at the angular rate α can be written as [27, App. C]

$$\sigma_\alpha^2 = \left(\frac{\alpha \cos\theta_e D_a}{2.54\pi}\right)^2 \ln 2 = \left(\frac{\alpha\lambda\cos\theta_e}{2\pi\theta_1}\right)^2 \ln 2 = \frac{\alpha^2\cos^2\theta_e}{16k^2\sigma_\theta^2}. \quad (2)$$

In (2), $\theta_{\rm e}$ is the elevation angle (it will be assumed smaller than 5°; therefore, $\cos\theta_{\rm e} \approx 1$), θ_1 is the 3-dB one-way power pattern beamwidth, λ is the wavelength, $k = 2\pi/\lambda$ is the wavenumber, σ_θ^2 is the second central moment of the two-way power pattern, and it is equal to $\theta_1^2/16\ln 2$ [27, Sec. 5.3].

OU-PRIME had a beam scanning at a rate of 16° s^{-1} and processed 38 signal samples spaced at the PRT equal to 847 μs; thus the dwell time $T_{\rm d} = 32.19$ ms. Given the 3-dB one-way beamwidth θ_1 equals to 0.5°, $\theta_{\rm e} \le 5^\circ$, and $\lambda = 5.44$ cm, σ_α is about 0.23 m s^{-1}. It will be assumed clutter is primarily from hard scatterers on the ground; that is, the *intrinsic* clutter spectrum is a delta function, and the *asymptotic* clutter spectrum width is equal to σ_α.

The *observed* clutter spectrum is the spectrum observed when the beam is scanning and actual data acquisition parameters are used. The *observed* clutter spectrum is the convolution of the *asymptotic* clutter spectrum and the spectrum associated with the Blackman window function. Thus, the expected width, $\Delta v_{\rm w}$, of the observed clutter is $\Delta v_w = \sqrt{\sigma_{\rm B}^2 + \sigma_\alpha^2}$. If the power spectrum of the Blackman window is $W(v)$, the square root of the second central moment $\sigma_{\rm B}^2$ of the power spectrum of Blackman window, numerically evaluated, can be approximated by

$$\sigma_{\rm B} = \sqrt{\frac{\int_{-v_{\rm N}}^{v_{\rm N}} v^2 W(v)dv}{\int_{-v_{\rm N}}^{v_{\rm N}} W(v)dv}} \approx \frac{0.34\lambda}{T_{\rm d}} \approx 0.58 \text{ m s}^{-1}. \quad (3)$$

From (3), it is evident $\sigma_{\rm B}$ is inversely proportional to the dwell time $T_{\rm d}$, and because $\sigma_\alpha = 0.23$, $\sigma_{\rm B} \approx 2.5\sigma_\alpha$. Because $T_{\rm d}$ and α values in this work are those typically used operationally and are fixed, $\Delta v_{\rm w}$ is a constant. Thus, the broadening effect of the Blackman window dominates the broadening effect due to beam scanning so $\Delta v_{\rm w} \approx \sigma_{\rm B}$.

2) SPD Distributions: In this section, the conditional probabilities of SPD are presented given separately the classes of clutter, narrow-band zero-velocity weather signals, and non-zero velocity weather signals. The conditional probability density functions (PDFs) of SPD for: 1) clutter, 2) narrow-band zero-velocity weather (i.e., $|v_{\rm rw}| \le 1$ m s^{-1}, $\sigma_{\rm vw} \le 1$ m s^{-1}, $\rho_{\rm hv} \ge 0.99$, and SNR ≥ 3 dB), and 3) non-zero velocity weather (i.e., $|v_{\rm rw}| > 1$ m s^{-1}, $\rho_{\rm hv} \ge 0.99$, and SNR ≥ 3 dB) are obtained from OU-PRIME data and shown in Fig. 2. The mean radial velocity is calculated by using the pulse pair processor [27, Sec. 6.4.1], and the spectrum width is calculated by using the ratio of autocovariances at lag 1 and 2 [27, Sec. 6.5.1]. Here, $\sigma_{\rm vw} \le 1$ m s^{-1} is chosen to define narrow-band weather spectra because such spectra are similar to clutter spectra, and it is challenging to distinguish one from the other, particularly if the weather has a near-zero Doppler velocity. $\rho_{\rm hv}$ is the zero lag copolar cross correlation coefficient [27, Sec. 6.8.5] which is only used to help distinguish weather spectra from clutter spectra in order to show separately the conditional PDFs of SPD for clutter and weather. Zrnić *et al.* [28] show only 17% of ground clutter data have $\rho_{\rm hv}$ larger than 0.97 when the scan rate is 15.8° s^{-1} and $\rho_{\rm hv}$ seldom falls below 0.9 in precipitation including hail. For stratiform rain, values of $\rho_{\rm hv}$ are close to unity [29]. Because the SCI as presently formulated applies to radar transmitting either H or V polarized waves (these radars are still used in many places), $\rho_{\rm hv}$ is not used in the current SCI algorithm.

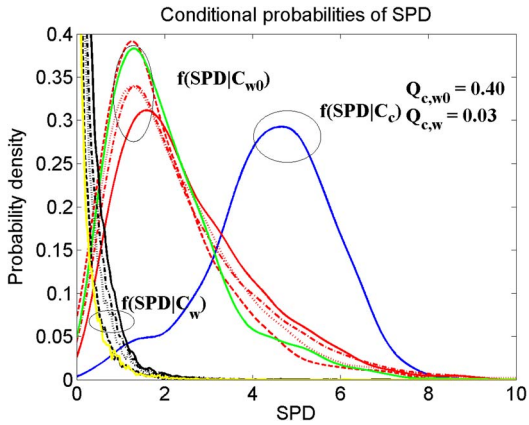

Fig. 2. Conditional PDFs for SPD given narrow-band zero-velocity weather signals, non-zero velocity weather signals, and clutter.

The SPD distribution for narrow-band zero-velocity and non-zero velocity weather signals in Fig. 2 are obtained from five stratiform weather days. Data which were collected at 18:02 UTC 10/21/2009, 05:10 UTC 01/21/2010, 13:08 UTC 04/17/2010, 09:07 UTC 05/13/2010, and 21:49 UTC 09/08/2010 with elevation angle $\theta_{\rm e} = 3.5^\circ$. Because $\theta_{\rm e} = 3.5^\circ$ and the beamwidth is 0.5°, there is practically no clutter present. Because a large number of data are needed to obtain reliable estimates of the PDFs, data from stratiform weather are chosen because such weather should provide an abundance of narrow-band weather signals.

Ground clutter data were collected at 15:47 UTC Aug 4th 2011 with $\theta_{\rm e} = 0.5^\circ$ under clear sky conditions. Time-series data for which CNR was larger than 30 dB and $|v_{\rm rc}| \le 1$ m s^{-1} was selected for analysis. The large CNR threshold is chosen to eliminate echoes from zero Doppler velocity biological scatterers that are likely present in August. The terrain surrounding

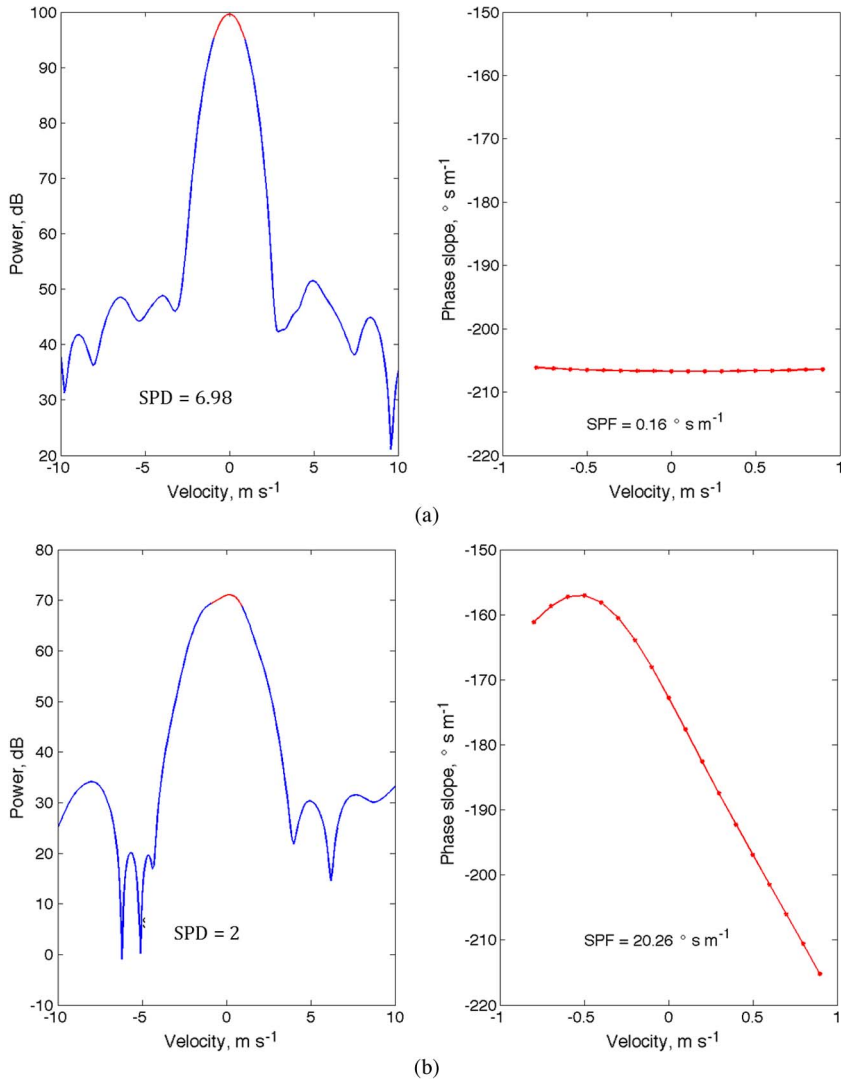

Fig. 3. Power spectrum $P(v)$ and spectral phase slope $a(v)$ within the spectral intervals ± 10 m s^{-1} and $\pm\sqrt{2}\Delta v_{\rm w}$, respectively. (a) Clutter spectrum from clutter data: $v_{\rm rc} = 0$, $\sigma_{\rm vc} = 0.8$ m s^{-1}, and $\rho_{hv} = 0.58$. The clutter data were collected at 23:19 UTC on 01/13/2011 under clear condition with $\theta_{\rm e} = 0$. (b) Narrow-band zero-velocity weather signal spectrum from stratiform weather data: $v_{\rm rw} = 0$, $\sigma_{\rm vw} = 1.0$ m s^{-1}, and $\rho_{hv} = 0.997$. The weather data were collected at 05:51 UTC on 12/02/2009 under stratiform precipitation condition with $\theta_{\rm e} = 3.5^{\circ}$.

OU-PRIME is a mixture of forest, prairie, and urban settings. Thus all types of clutter (except sea clutter) are being sampled. The August case represents ground conditions when there is full foliage.

In Fig. 2, the conditional PDF given clutter (i.e., $f(\text{SPD}|C_{\rm c})$, the capital "C" represents class and the subscript "c" represents clutter) collected in August 4th under clear air conditions, and those given narrow-band zero-velocity (i.e., $f(\text{SPD}|C_{\rm w0})$, the subscript "w0" represents narrow-band zero-velocity weather signals) and non-zero velocity weather signals (i.e., $f(\text{SPD}|C_{\rm w})$, the subscript "w" represents non-zero velocity weather signals) collected in five days in January, April, May, September, and October with stratiform precipitations are shown. The density functions are smoothed by the Gaussian kernel [11]. Fig. 2 suggests SPD can distinguish a large percentage of clutter from narrow-band zero-velocity weather signals. The numerical entries, $Q_{\rm c,w0}$, etc. in Fig. 2, represent the common area (i.e., the area under the minimum of the two curves) between the mean (i.e., the average of PDFs obtained from five days of observation) conditional PDFs given the various classes; a smaller common area indicates better discrimination. For example, $Q_{\rm c,w0} = 0.40$ and $Q_{\rm c,w} = 0.03$ demonstrate it is more difficult to distinguish ground clutter from narrow-band zero-velocity weather signals.

B. SPF

In this section, SPF is defined, and its conditional PDFs are given for the three data classes. Numerical simulations and theory show the spectral phase $\xi(v)$ of clutter from a hard scatterer has a linear dependence on v, but the spectral phase of weather signal is a random function of v. Thus, the linearity of spectral phase in the spectral interval $\pm\sqrt{2}\Delta v_{\rm w}$ could also be a good discriminant to distinguish clutter from weather signals.

In order to have more spectral phase data points within the interval $\pm\sqrt{2}\Delta v_{\rm w}$ to compute SPF, zero padding to the time-series data is applied after the window function. It is stated that zero padding in the time domain corresponds to *ideal interpolation* in the frequency domain [30]. The SPF was applied with and without zero padding, and it was found the skill of SPF

increased with zero padding. Without zero padding only three spectral lines are within $\pm\sqrt{2}\Delta v_{\rm w}$, but with zero padding, there are 18 spectral lines. SPF calculates the standard deviation (SD) of the phase slope $a(v)$ within the spectral interval. The SPF is defined as

$$\text{SPF} = \text{SD}\left[a(v)\right] = \text{SD}\left[\frac{\xi(v) - \xi(v-\Delta v)}{\Delta v}\right], \quad v \in \left[-\sqrt{2}\Delta v_{\rm w} + \Delta v : \sqrt{2}\Delta v_{\rm w}\right]. \quad (4)$$

The phase term $\xi(v)$ is unwrapped to avoid that the absolute jump between consecutive phase elements that is larger than or equal to $\pm\pi$. In (4), Δv is the spectral interval between adjacent bins, and it is equal to 0.1 m s^{-1}. SPF measures how much the phase within the spectral interval $\pm\sqrt{2}\Delta v_{\rm w}$ deviates from a line. If all the phase elements within the spectral interval are on a line, SPF is equal to zero. SPF is small for clutter, but larger if the weather spectrum overlays the clutter spectrum within $\pm\sqrt{2}\Delta v_{\rm w}$. Examples of the power spectrum $P(v)$ and spectral phase slope $a(v)$ from real data are shown in Fig. 3.

If the phase $\xi(v)$ in the spectral interval $\pm\sqrt{2}\Delta v_{\rm w}$ has a linear slope, the phase slope $a(v)$ in this spectral interval should be a constant. As can be seen from Fig. 3(a), the spectral phase slope of clutter is almost a constant in the spectral interval but that of narrow-band zero-velocity weather signal is not. SPF is equal to 0.16° s m^{-1} in Fig. 3(a) and 20.26° s m^{-1} in Fig. 3(b). In addition, SPF is calculated for the simulated spectra shown in Fig. 1.

In Figs. 1(a) and (b), SPF is, respectively, equal to 2.1 and 33.7° s m^{-1}, and these results suggest the SPF has the capability of distinguishing clutter from narrow-band zero-velocity weather signals. In Fig. 1(c) and (d), SPF is respectively equal to 2.1 and 2.8° s m^{-1}, both of which are small, which means SPF is almost not affected by CSR when $v_{\rm rw}$ is equal to -10 m s^{-1} (i.e., the spectral power of clutter is dominant in the spectral interval $\pm\sqrt{2}\Delta v_{\rm w}$); In Fig. 1(e) and (f), SPF is, respectively, equal to 7.0 and 58.8° s m^{-1}, which means if the spectra of clutter and weather signal are overlapped and the weather power is dominant in the spectral interval $\pm\sqrt{2}\Delta v_{\rm w}$, the phase of the spectral elements within $\pm\sqrt{2}\Delta v_{\rm w}$ do not have a linear dependence on Doppler velocity. The conditional PDFs of SPF given clutter $f(\text{SPF}|C_{\rm c})$, narrow-band zero-velocity weather signals $f(\text{SPF}|C_{\rm w0})$, and non-zero velocity weather signals $f(\text{SPF}|C_{\rm w})$ are shown in Fig. 4.

From Fig. 4, it can be seen that the conditional PDF given weather signals has long tails, which is related to the fact that spectral phase in the interval $\pm\sqrt{2}\Delta v_{\rm w}$ fluctuates randomly. On the other hand, the conditional PDF given clutter would be almost a delta function centered at zero if there is only one hard scatterer in the resolution volume (i.e., the phase within the interval $\pm\sqrt{2}\Delta v_{\rm w}$ would almost be linear). The reason that the PDF is far away from a delta function can be explained by the fact that there are multiple hard scatterers being scanned by the radar.

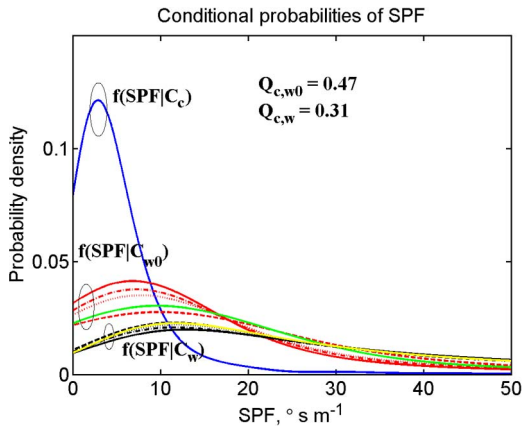

Fig. 4. Conditional PDFs of SPF given narrow-band zero-velocity weather signals, non-zero velocity weather signals, and clutter. The weather and clutter data are from the same data sets stipulated in Fig. 2.

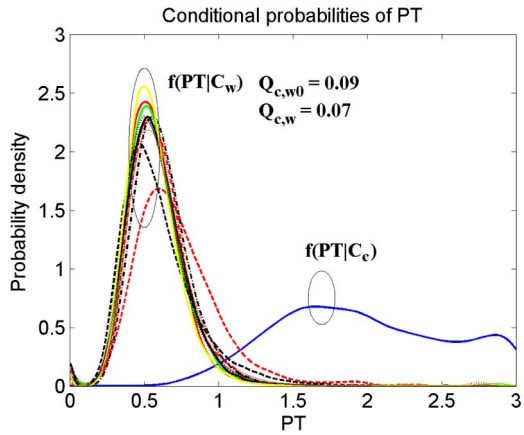

Fig. 5. Conditional PDFS of PT given clutter and weather (narrow-band zero-velocity and non-zero velocity signals). The weather and clutter data are from the same data sets stipulated in Fig. 2.

C. PT

In this section, PT is defined and its conditional PDFs are given for the three classes. In this paper, the definition of texture is different from the one defined in [5]. The texture in [5] is defined as the mean of the squared reflectivity difference between adjacent gates whereas the definition of texture in this paper is given by (5). The discriminant PT takes advantage of the fact that the mean power of weather signals is spatially more uniform than the mean power of clutter. PT is defined as

$$\text{PT}_{i,j} = \frac{\text{SD}[P_{i,j-L:j+L}]}{\text{MEAN}[P_{i,j-L:j+L}]}. \quad (5)$$

$\text{PT}_{i,j}$ is the PT at azimuth ϕ_i and range r_j. The SD of power about its mean is calculated along the range for nine gates (i.e., $L = 4$) centered on gate i, j. In Fig. 5, the conditional PDFs of PT given ground clutter and weather are shown.

One thing to notice is that unlike the SPD and SPF, the conditional PDFs of PT $f(\text{PT}|C_{\rm w0})$ and $f(\text{PT}|C_{\rm w})$ are very similar (also true for SWT shown in Section II-D). Thus, $f(\text{PT}|C_{\rm w})$ is used in Fig. 5 to represent both $f(\text{PT}|C_{\rm w0})$ and $f(\text{PT}|C_{\rm w})$. The common area between clutter and narrow-band zero-velocity weather signals is equal to 0.07 which is much smaller than those for SPD (0.40) and SPF (0.47). Thus, PT outperforms

SPD and SPF in distinguishing clutter from narrow-band zero-velocity weather signals. The disadvantage of using PT or SWT is that it will increase the number of false positives (FPs) (i.e., weather signals mistakenly identified as clutter). For example, if only one gate is contaminated by strong ground clutter, all nine range gates centered on the clutter gate could be tagged as having significant clutter even if there is no clutter. On the other hand, because the SPD discriminant is applied first (Fig. 7), and if SPD < 0.03, data from that gate will tagged as weather and thus data from this gate will not be falsely tagged by the PT discriminant as having significant clutter.

D. SWT

In this section, SWT is defined and its conditional PDFs are given for the three classes. Fang *et al.* [31] pointed out that the spectrum width has significant error if the in-trip echo power is less than 20 dB stronger than the sum of out-of-trip echo powers. Applied to our case, it means that even if CSR is as small as -20 dB, the spectrum width of weather signal can have significant bias (Table III). Ground clutter power is spatially variable compared to weather echo power and this is the reason why PT is an effective discriminant if the clutter power is dominant. However, if CSR is smaller than 0 dB, PT becomes less effective and clutter detection becomes difficult as noted by [5]. On the other hand, estimated spectrum widths of weather signals can be significantly biased by clutter power, particularly if the mean radial velocity of weather signal is far from zero. In this case, SWT can be useful both when the CSR is low or high. However, when the radial velocity of weather signal is small and CSR is large, analysis has shown SWT is not as effective as PT.

For narrow-band weather signals and SNR > 15 dB, the absolute power differences (APD) spectrum width estimator has better performance than the more commonly used estimators [32]. The APD spectrum width estimator is

$$\hat{\sigma}_v = \frac{\lambda}{4\pi T_\mathrm{s}} \ln^{\frac{1}{2}} \frac{1}{\left(1-\left(\frac{\Delta\hat{P}(T_\mathrm{s})}{\hat{P}}\right)^2\right)\left(\frac{\hat{P}}{\hat{P}-\overline{N}}\right)^2} \tag{6a}$$

$$\Delta\hat{P}(T_\mathrm{s}) = \frac{1}{M-1}\sum_{k=1}^{M-1} |P_{k+1}-P_k| \tag{6b}$$

$$\hat{P} = \frac{1}{M}\sum_{k=1}^{M} P_k \tag{6c}$$

where the diacritical hat $\wedge$ defines an estimate. M is the number of samples per dwell time T_d. The estimated power $\hat{P}$ is equal to the summation of signal power $\hat{S}$, clutter power $\hat{C}$, and average noise power $\overline{N}$. $\overline{N}$ is estimated with many more samples than that used to estimate $\hat{P}$ and is the reason for the overbar above N. The average noise power can be estimated by the gates (usually far from the radar) that only contain noise power. The definition of SWT is the same as PT shown in (5) except power P is changed to spectrum width σ_v.

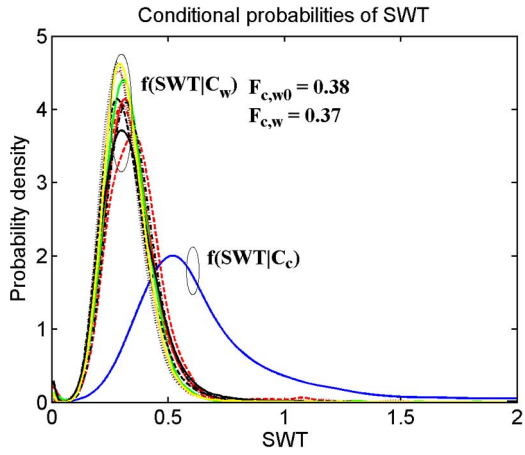

Fig. 6. Conditional PDFs of SWT given narrow-band zero-velocity weather signals, non-zero velocity weather signals, and clutter. The weather and clutter data are from the same data sets stipulated in Fig. 2.

In Fig. 6, the conditional PDFs of SWT given clutter $f(\mathrm{SWT}|C_\mathrm{c})$, narrow-band zero-velocity weather signals $f(\mathrm{SWT}|C_{\mathrm{w}0})$, and non-zero velocity weather signals $f(\mathrm{SWT}|C_\mathrm{w})$ are shown. Because it is difficult to distinguish $f(\mathrm{SWT}|C_{\mathrm{w}0})$ and $f(\mathrm{SWT}|C_\mathrm{w})$, $f(\mathrm{SWT}|C_\mathrm{w})$ is used to represent both $f(\mathrm{SWT}|C_{\mathrm{w}0})$ and $f(\mathrm{SWT}|C_\mathrm{w})$ in Fig. 6. The common area between clutter and narrow-band zero-velocity weather signals is equal to 0.38 which is larger than that for PT (0.07) and almost the same with that for SPD (0.40) but smaller than that for SPF (0.47).

E. Implementation Procedures

In this section, the four discriminants are combined by using the SBC. Figs. 2 and 4 indicate that it is more difficult to distinguish ground clutter from narrow-band zero-velocity weather signals than from non-zero velocity weather signals. Thus, if ground clutter can be distinguished from narrow-band zero-velocity weather signals, it can be distinguished from all other kinds of weather signals. Therefore, using the SBC, only two classes, C_c (ground clutter) and $C_{\mathrm{w}0}$ (narrow-band zero-velocity weather signals), are considerd. By doing so, the algorithm can be simplified. $\boldsymbol{X}$ represents the 4-D attribute vector, $\boldsymbol{X} = (\mathrm{SPD}, \mathrm{SPF}, \mathrm{PT}, \mathrm{SWT})$. For the current gate, $\boldsymbol{X} = \mathrm{X_O}$ (subscript "O" represents the observed discriminants). The SBC judges whether the $\boldsymbol{X} = \boldsymbol{X}_\mathrm{O}$ belongs to C_c or $C_{\mathrm{w}0}$. $\boldsymbol{X} = \boldsymbol{X}_\mathrm{O}$ belongs to C_c only if $f(C_\mathrm{c}|\boldsymbol{X} = \boldsymbol{X}_\mathrm{O}) > f(C_{\mathrm{w}0}|\boldsymbol{X} = \boldsymbol{X}_\mathrm{O})$. According to Bayes' theorem [33, ch. 7-3]

$$f(C_\mathrm{i}|\boldsymbol{X} = \boldsymbol{X}_\mathrm{O}) = \frac{f(\boldsymbol{X} = \boldsymbol{X}_\mathrm{O}|C_\mathrm{i})f(C_\mathrm{i})}{f(\boldsymbol{X} = \boldsymbol{X}_\mathrm{O})}; \quad i = c, \quad w0. \tag{7}$$

$f(\boldsymbol{X} = \boldsymbol{X}_\mathrm{O}) \equiv K$ is the probability the observation $\boldsymbol{X}_\mathrm{O}$ occurs and is the same for both classes. Thus $f(C_\mathrm{i}|\boldsymbol{X} = \boldsymbol{X}_\mathrm{O})$ is proportional to $f(\boldsymbol{X} = \boldsymbol{X}_\mathrm{O}|C_\mathrm{i})f(C_\mathrm{i})$. Because the PDFs $f(C_\mathrm{c})$ and $f(C_{\mathrm{w}0})$ are not known a priori, both classes are assumed equally likely (i.e., $f(C_\mathrm{c}) = f(C_{\mathrm{w}0}) = 0.5$). Then, the SBC is

$$f(C_\mathrm{i}|\boldsymbol{X} = \boldsymbol{X}_\mathrm{O}) = 0.5K^{-1}f(\boldsymbol{X} = \boldsymbol{X}_\mathrm{O}|C_\mathrm{i}). \tag{8}$$

Thus, the SBC assigns $\boldsymbol{X} = \boldsymbol{X}_0$ to C_c only if $f(\boldsymbol{X} = \boldsymbol{X}_O|C_c) > f(\boldsymbol{X} = \boldsymbol{X}_O|C_{w0})$. To shorten notation, f_c and f_{w0} are used to represent $f(\boldsymbol{X} = \boldsymbol{X}_O|C_c)$ and $f(\boldsymbol{X} = \boldsymbol{X}_O|C_{w0})$. $f(\boldsymbol{X}|C_i)$ can be written as

$$f(\boldsymbol{X}|C_i) = f(\text{SPD} \cap \text{SPF} \cap \text{PT} \cap \text{SWT}|C_i). \tag{9}$$

In the SBC, the simple assumption of class-conditional independence is made [34, ch. 8.3.2]. It is also found that the four discriminants can be considered as class-conditional independent by using a method similar to chi-square test [33, ch. 9-3]. Thus

$$f(\boldsymbol{X}|C_i) = f(\text{SPD}|C_i) f(\text{SPF}|C_i) f(\text{PT}|C_i) f(\text{SWT}|C_i). \tag{10}$$

The conditional PDFs of SPD SPF, SWT, and PT, given class label C_i can be obtained from ground truth (i.e., clutter data obtained in clear air conditions and weather data obtained at high elevation angles) as given in Figs. 2, 4–6, respectively. Thus, the joint conditional PDF $f(\boldsymbol{X}|C_i)$ can be calculated for each class. One needs to be aware that $f(\boldsymbol{X}|C_i)$ is dependent on the radar sites, radar characteristics, scan strategies, and environmental conditions.

The algorithm is divided in the following steps:

1) Calculate SCNR. If SCNR $>$ 3 dB, go to step 2), otherwise the current gate is considered not to have significant weather; then compute SCNR for the next range gate.
2) Apply the Blackman window function and then add zeros to the time-series data.
3) Compute SPD. If SPD > 0.03, go to step 4), otherwise, the current gate is considered not clutter contaminated. This SPD threshold reduces the number of FPs (Section III-A) caused by the texture discriminants; the threshold of 0.03 corresponds to a CSR equal to -15 dB (Section II-A).
4) Compute SPF, PT, and SWT. Look up the joint conditional PDF $f(\boldsymbol{X}|C_i)$ obtained from ground truth. Calculate f_c and f_{w0}.
5) If $f_c > f_{w0}$ the current gate, data is clutter contaminated, otherwise, data are not contaminated; then return to step 1) for the next gate.

Steps 1 through 5 are shown in a flow chart (Fig. 7).

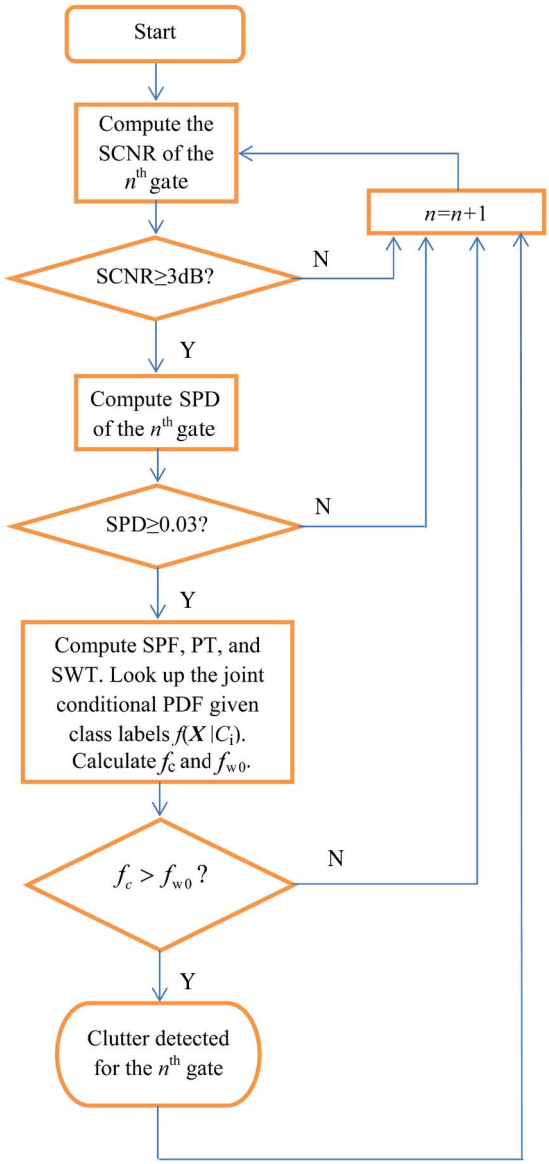

Fig. 7. Flow chart of the implementation procedures of the SCI algorithm.

III. Clutter Detection Performance Based on Controlled Synthesized Data

The SCI algorithm was tested on four different data sets which are the combination of one clutter data set, collected with $\theta_e = 0^\circ$ and under clear air winter conditions (i.e., at 23:19 UTC on 01/13/2011), and four weather data sets, collected with $\theta_e = 3.5^\circ$ and under stratiform rain conditions at 07:04 UTC on 04/12/2009, 05:51 UTC on 12/02/2009, 04:55 UTC on 04/18/2010, and 12:33 UTC on 05/14/2010. Clutter data collected in winter minimize the number of airborne biological scatterers that could contaminate the clutter field. In order to quantify the performance of SCI, recorded clutter I/Q data is added to I/Q data from stratiform weather. By doing so, the locations contaminated by ground clutter, as well as the CSRs of the contaminated gates, are known. Furthermore, only clutter data having CNR $\geq$ 30 dB and $|v_{rc}| \leq 1$ m s^{-1} are used to provide clutter not contaminated from insects that have zero radial velocities. Likewise, collecting weather echoes at elevation angles several beam widths above the horizon better insures that the weather data are not contaminated with ground clutter. The synthesized data with CSR smaller than -15 dB are considered as pure weather because the bias caused by ground clutter is so small that can be neglected as can be inferred from Table III. Thus, the contaminated gates are those with CSR no less than -15 dB.

Stratiform weather data were collected to have many weather spectra with small spectrum widths and mean Doppler velocities near zero. The horizontal reflectivity (Z_h), mean radial velocity (v_r), spectrum width (σ_v), and SNR for one of the weather data sets (i.e., on 12/02/2009), are displayed in Fig. 8 to a range of 50 km, a range interval over which clutter detection performance was evaluated. The Z_h field is mostly uniform, but shows a ring of enhanced reflectivity suggestive of a melting

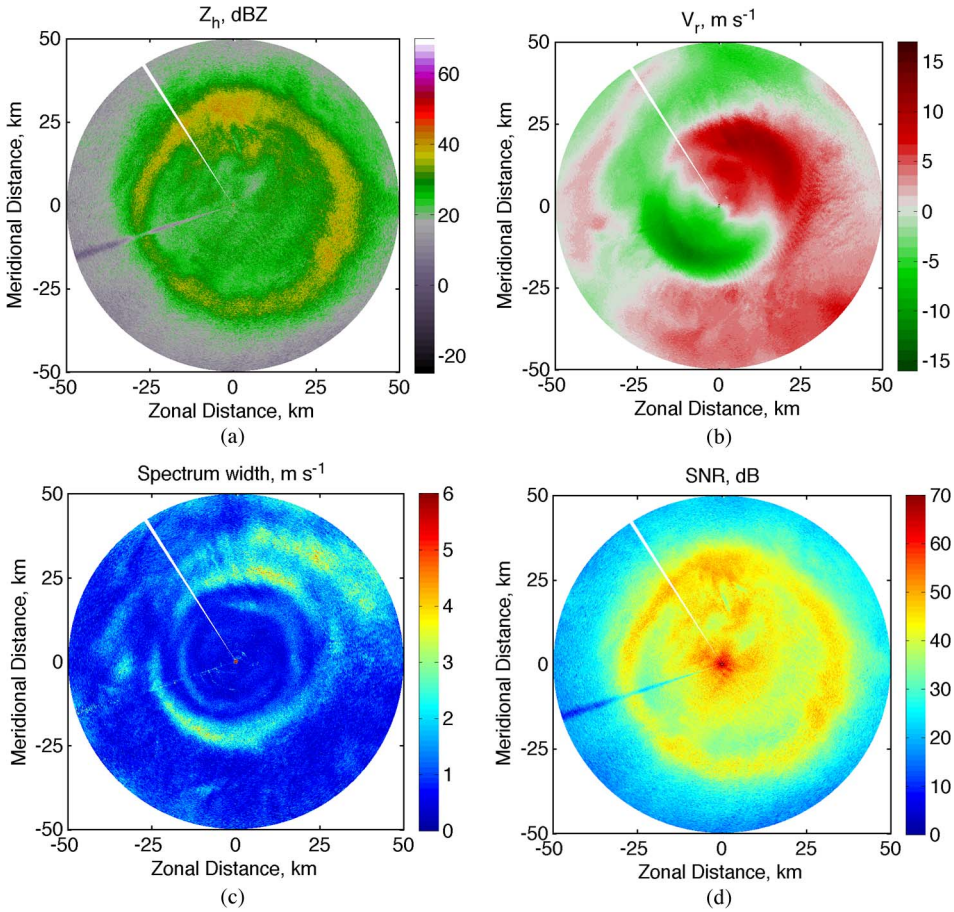

Fig. 8. (a) Horizontal reflectivity. (b) Radial velocity. (c) Spectrum width. (d) SNR. The stratiform rain data were collected at 05:51 UTC, December 2, 2009 with $\theta_e = 3.5°$.

layer. The σ_v field is also mostly uniform and reveals, near the bottom of the melting layer, a feature of enhanced width suggestive of a layer of shear and/or turbulence. About 24% of the zero-velocity weather signals ($|v_{rw}| \leq 1$ m s^{-1}) have the spectrum width less than 1 m s^{-1}.

In order to combine clutter and weather signal data, recorded clutter I/Q data are added to the I/Q data obtained from stratiform weather. An example of the outcome of this synthesis procedure is shown in Fig. 9. In the contaminated gates, the reflectivity increases [Fig. 9(a)] and the radial velocity is biased toward zero [Fig. 9(b)] and the spectrum width is biased high in most contaminated gates [Fig. 9(c)]. Fig. 9(d) presents the map of CSR.

In Fig. 10, the PDF of CSR is shown for all the gates where ground clutter was added to the weather signals.

A. Evaluating the Performance of SCI

SCI is applied to the four synthesized data sets. Data sets used to obtain the conditional PDFs shown in Figs. 2, 4–6 are not used in the testing process to avoid the overoptimistic estimates due to overspecialization of the learning algorithm to the data [34, ch. 8.5]. In Fig. 11, $\log_{10}(f_c)$ and $\log_{10}(f_{w0})$, obtained from the SCI algorithm, are shown.

Fig. 11(a) gives the probability that clutter is present in each gate whereas Fig. 11(b) is the probability there is only narrowband zero-velocity weather signal. By comparing f_c with f_{w0}, a decision can be made as to whether significant clutter is present in each of the locations where ground clutter was inserted. It can be seen from Fig. 11(b) that the zero velocity regions are remarkably delineated by f_{w0}.

To evaluate the clutter detection performance of the SCI, the probability of detection (POD) and the false alarm rate (FAR) are computed. The definitions of POD and FAR are [34, ch. 8.5.1]

$$\text{POD} = \frac{\text{True Positives}}{\text{True Positives} + \text{False Negatives}} \tag{11a}$$

$$\text{FAR} = \frac{\text{False Positives}}{\text{False Positives} + \text{True Negatives}} \tag{11b}$$

In (11), "Positive" labels the location that the detector judges as clutter contaminated, and "Negative" labels the location that the detector judges as weather; "True Positive (TP)" labels the location that 1) the detector judges as clutter contaminated and 2) true CSR ≥ -15 dB; "False Negative (FN)" denotes the location that 1) the detector judges as weather, and 2) true CSR ≥ -15 dB; "False Positive (FP)" denotes the location that 1) the detector judges as clutter and 2) true CSR < -15 dB; "True Negative (TN)" denotes the location that 1) the detector judges as weather and 2) true CSR < -15 dB.

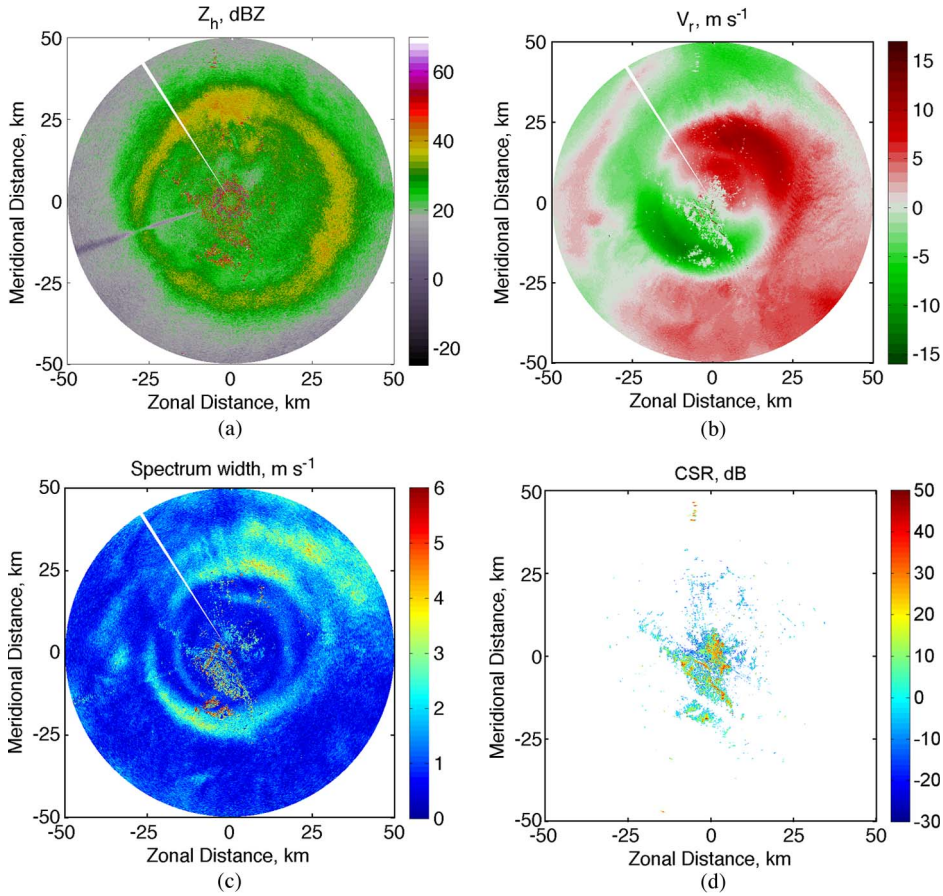

Fig. 9. Weather signals (12/02/2009) mixed with clutter (01/13/2011). (a) Horizontal reflectivity. (b) Radial velocity. (c) Spectrum width. (d) CSR.

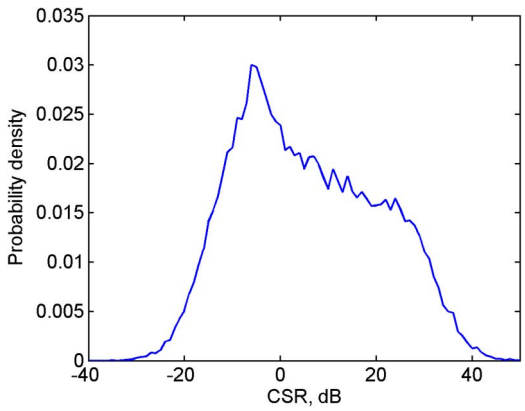

Fig. 10. PDF of CSR for the composite data of weather (12/02/2009) and clutter (01/13/2011).

SCI performance is evaluated by comparing PODs and FARs with that obtained using the bench mark results from application of the CMD algorithm (presently used by the USA's national network of Doppler weather radars to detect clutter) applied to the same data. The CMD code CMD AEL V4.1 was received from NWS' Radar Operation Center (ROC). Fig. 12 shows the performance of SCI and CMD in detecting clutter in the synthesized data field of Fig. 9. The clutter ground truth is given in Fig. 12(c). It can be seen that SCI has more correct detections and less number (2950 versus 3849) of FPs than that reported by CMD in regions beyond 25 km where there is no clutter. The number of TNs is about equal (241891 and 240992). The POD for all the clutter contaminated gates having CSR larger than -15 dB is equal to 72.25% and 61.39% for the SCI and CMD, respectively; and the FAR for all the non-contaminated gates is equal to 1.2% and 1.57%, respectively. The reason the FAR is low is because the TN in the denominator of (11b) is very large.

In Table IV, TP, FN, FP, FN, POD, and FAR of the four synthesized data are summarized for SCI and CMD, respectively. From Table IV, it can be inferred the POD of SCI is more than 10% higher than that of CMD for all the four cases. However, the FAR of SCI is about the same as that for CMD.

Fig. 13 gives the POD, obtained from four synthesized data sets, as a function of CSR for CSR larger than -15 dB. For example, in order to obtain the PODs using SCI and CMD algorithms at CSR $= 0$ dB, all the gates contaminated by ground clutter having CSR larger than -0.5 dB but smaller than 0.5 dB are counted and summed to give the true number (i.e., N_{true}) of gates having CSR $= 0$ dB. Next, sum the number (i.e., N_{SCI} or N_{CMD}) of clutter contaminated (i.e., for CSR $= 0$ dB) gates detected by SCI or CMD. The ratios $N_{\text{SCI}}/N_{\text{true}}$ and $N_{\text{CMD}}/N_{\text{true}}$ are the PODs using SCI and CMD algorithm for CSR $= 0$ dB.

The SCI's POD is significantly higher than that for the CMD at CSR < 5 dB. This better performance is caused by discriminants SPF and SWT continuing to be effective at low

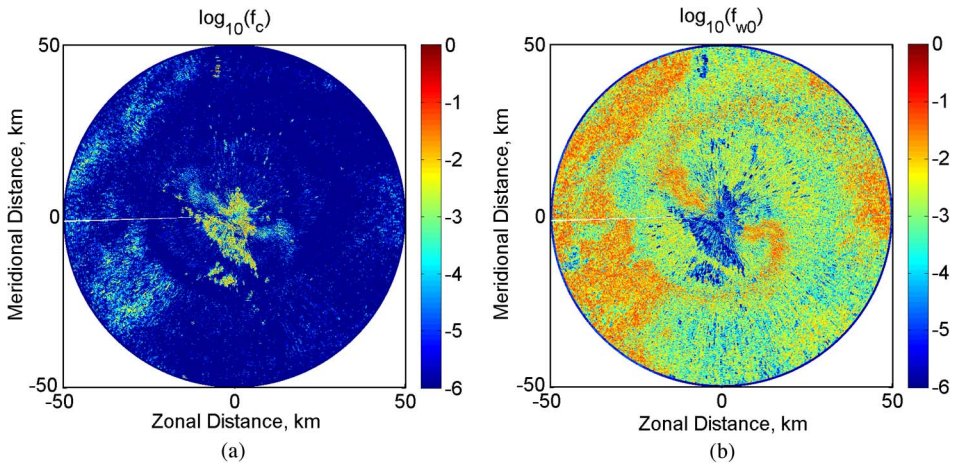

Fig. 11. Joint conditional probability density values in logarithm units given (a) clutter and (b) narrow-band zero-velocity weather signals. The data are from the same data set shown in Fig. 9.

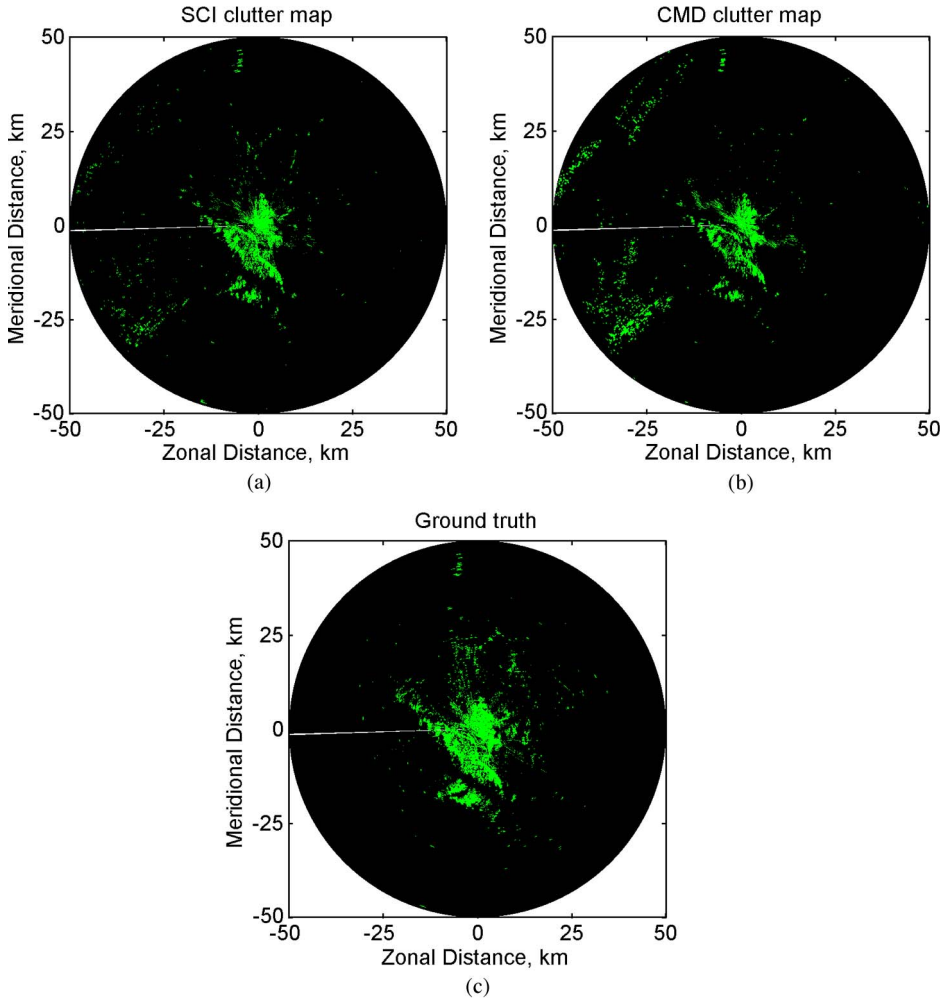

Fig. 12. Clutter detection maps for weather signals mixed with clutter shown in Fig. 9. (a) SCI clutter map. (b) CMD clutter map. (c) Ground truth CSR ≥ -15 dB.

CSR if weather and clutter are not overlapped (Sections II-B and II-D). However, most of the higher POD is due to SWT; the SPF discriminant increases the PODs by less than a few percent. The better performance at low CSR is due to the fact that there are many more locations where spectra of weather and clutter are not overlapped and these are the conditions under which SWT is most effective. If CSR > 5 dB, the SCI shows small improvement in POD (smaller than 10%) over the bench mark results obtained with CMD. This slightly better performance is caused by the discriminant SPD which has a better capability than the CPA to distinguish ground clutter from narrow-band zero-velocity weather signals.

TABLE IV
PERFORMANCES OF SCI AND CMD ALGORITHM BASED ON FOUR SYNTHESIZED DATA

	TP SCI/CMD	FN SCI/CMD	FP SCI/CMD	TN SCI/CMD	POD SCI/CMD	FAR SCI/CMD
04/12/2009	22630/16734	11121/17017	3127/2130	251122/252119	67.05%/49.58%	1.23%/0.84%
12/02/2009	31181/26497	11978/16662	2950/3849	241891/240992	72.25%/61.39%	1.2%/1.57%
04/18/2010	31982/27074	11054/15962	4193/4522	240771/240442	74.31%/62.91%	1.71%/1.85%
05/14/2010	32458/27651	10980/15787	2926/2688	241636/241874	74.72%/63.66%	1.2%/1.1%

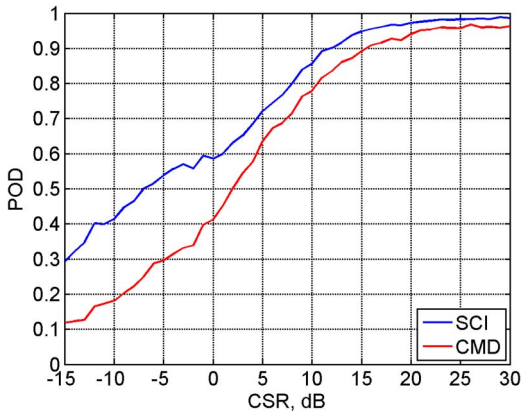

Fig. 13. Comparison between the POD of clutter mixed with weather signals using SCI and CMD algorithms as a function of CSR. Results are obtained from four synthesized data sets.

The POD for CMD in Fig. 13 is smaller than that presented by [5, Fig. 6] even though data for both figures were obtained from stratiform weather. A possible explanation for this apparent discrepancy is that [5] estimates CSR by comparing power in the spectrum before and after applying GMAP, whereas in constructing Fig. 13, precise CSR is obtained from the synthesized mixed clutter and weather signals. Thus, in [5], clutter residuals after filtering is attributed to weather signals and this decreases the estimate of CSR which, in turn, causes the true POD to be shifted to lower CSR showing POD larger than the true POD. In addition, the clutter data presented in [5] were collected in the Rocky mountain front range area, while the clutter data presented in this paper were collected in the terrain surrounding OU-PRIME which is a mixture of forest, prairie, and urban settings. Mountain type clutter is easier to identify because most clutter spectral power is almost a delta function at zero Doppler velocity.

IV. SUMMARY AND CONCLUSION

The SCI clutter detection algorithm is designed to detect ground clutter mixed with weather signals, even if the CSR is low but clutter can significantly bias weather spectral moment estimates (Table III). SCI combines the discriminants SPD, SPF, PT, and SWT using a SBC to detect clutter mixed with weather signals.

The conditional PDFs, PDFs, versus the levels of the various discriminants for practically pure ground clutter and pure narrow-band zero-velocity and non-zero velocity weather signals are obtained from clutter and stratiform weather data collected by OU-PRIME. The methodology used to collect practically pure clutter and weather signal data is described in Section II-A2. It is shown (Fig. 2) that the common area $Q_{\mathrm{c,w}}$ between the minimum of the PDFs curves for clutter and non-zero velocity weather signals is about 0.03 for the SPD discriminant. The common area is a measure of the discriminant's capability to distinguish various classes of clutter and weather. This small $Q_{\mathrm{c,w}}$ (ideally $Q_{\mathrm{c,w}} = 0$) suggests SPD is effective in detecting clutter mixed with non-zero velocity weather signals. However, the common area, $Q_{\mathrm{c,w0}}$, for narrow-band zero-velocity weather signals is significantly larger (Fig. 2) demonstrating the difficulty to distinguish this class of weather signals from clutter.

In order to improve the performance of SCI to detect clutter mixed with weather signals, a SPF discriminant has been added to the SCI. If a single fixed scatterer generates clutter, the spectral phase is linear in the spectral interval $\pm\sqrt{2}\Delta v_{\mathrm{w}}$ independent of the position of the scatterer within the radar's resolution volume. Departure from linearity is the basis to use spectral phase to detect stratiform weather signals mixed with clutter. However, it is found that the SPF discriminant improves the POD by only a few percent. This small improvement is due to clutter not typically being from a collection of scatterers where one scatterer is dominant.

The texture discriminants PT and SWT are both used in the SCI algorithm. PT effectively recognizes clutter when CSR is high (e.g., > 0 dB) whereas SWT recognizes clutter when CSR is low (e.g., -15 to 0 dB). Because the SWT is most effective if the Doppler velocity is at the Nyquist velocity, and because evaluation of clutter detectors was made using data collected by OU-PRIME, a 5-cm radar, it is expected the SWT discriminant will be more effective for 10-cm radars that have twice as large a Nyquist velocity.

One problem in evaluating the performance of clutter detectors is having reliable ground truth. To provide this ground truth, practically pure stratiform weather and clutter data were synthesized to obtain a data field of clutter mixed with weather as also suggested by [14]; in this case CSR is precisely known (Section III). This synthesis procedure provides quantitative estimates of CSRs to evaluate POD and FAR, and it was applied to four cases of stratiform weather (Table IV and Fig. 13). It is concluded SCI outperforms the CMD mostly in the low CSR (CSR < 5 dB, Fig. 13).

Although these preliminary results are promising, the SCI should be evaluated using other types of weather. On the other hand, detecting clutter in stratiform weather signals is the most challenging, and thus it is anticipated that SCI should work as well, if not better, for other types of weather. Furthermore, although the terrain surrounding OU-PRIME represents clutter from urban, wooded, and prairie regions, future study should address the performance of SCI to detect clutter from heavily foliage woods under different wind conditions.

ACKNOWLEDGMENT

The authors would like to acknowledge the useful advice provided by Dr. S. Torres from CIMMS (NOAA Cooperative Institute for Mesoscale and Meteorological Studies) and Mr. R. Ice from ROC during the review stage. The remarkably good comments and suggestions provided by three anonymous reviewers improved the quality of this paper. Many thanks go to staff of ARRC for maintaining the OU-PRIME radar and collecting data.

REFERENCES

[1] P. Meischner, *Weather Radar Principles and Advanced Applications*. Berlin, Germany: Springer-Verlag, 2002.

[2] R. Lee, G. Deruna, and J. Joss, "Intensity of ground clutter and of echoes of anomalous propagation and its elimination," in *Proc. 27th Conf. Radar Meteorol.*, Vail, CO, 1995, pp. 651–652.

[3] C. Kessinger, S. Ellis, and J. V. Andel, "The radar echo classifier: A fuzzy logic algorithm for the WSR-88D," presented at the 3rd Conf. Artificial Intelligence Applications Environmental Science, Long Beach, CA, 2003, P 1.6.

[4] J. C. Hubbert, M. Dixon, S. M. Ellis, and G. Meymaris, "Weather radar ground clutter. Part I: Identification, modeling, and simulation," *J. Atmos. Ocean. Technol.*, vol. 26, no. 7, pp. 1165–1180, 2009.

[5] J. C. Hubbert, M. Dixon, and S. M. Ellis, "Weather radar ground clutter. Part II: Real-time identification and filtering," *J. Atmos. Ocean. Technol.*, vol. 26, no. 7, pp. 1181–1197, 2009.

[6] R. L. Ice, R. D. Rhoton, J. C. Krause, D. S. Saxion, O. E. Boydstun, A. K. Heck, J. N. Chrisman, D. S. Berkowitz, and W. D. Zittel, "Automatic clutter mitigation in the WSR-88D, design, evaluation, and implementation," presented at the 34th Conf. Radar Meteorology, Williamsburg, VA, 2009, Paper 5.3.

[7] S. Torres, D. Warde, and D. S. Zrnić, *Signal design and processing techniques for WSR-88D ambiguity resolution: Part 15, the CLEAN-AP filter*, NSSL, Norman, OK. [Online]. Available: http://cimms.ou.edu/rvamb/Documents/Report_15.pdf

[8] D. Warde and S. Torres, "A novel ground-clutter-contamination mitigation solution for the NEXRAD network: The CLEAN-AP filter," presented at the Preprints, 26th Int. Conf. Interactive Information Processing Systems (IIPS) Meteorology, Oceanography, Hydrology, Atlanta, GA, 2010, Paper 8.6.

[9] A. D. Siggia and R. E. Passarelli, "Gaussian model adaptive processing (GMAP) for improved ground clutter cancellation and moment calculation," in *Proc. 3rd ERAD*, Visby, Sweden, 2004, pp. 67–73.

[10] G. Zhang, Y. Li, R. J. Doviak, D. Priegnitz, J. Carter, and C. D. Curtis, "Multipatterns of the national weather radar testbed mitigate clutter received via sidelobes," *J. Atmos. Ocean. Technol.*, vol. 28, no. 3, pp. 401–409, Mar. 2011.

[11] J. J. Gourley, P. Tabary, and J. P. D. Chatelet, "A fuzzy logic algorithm for the separation of precipitating from nonprecipitating echoes using polarimetric radar observations," *J. Atmos. Ocean. Technol.*, vol. 24, no. 8, pp. 1439–1451, Aug. 2007.

[12] H. Park, A. V. Ryzhkov, D. S. Zrnić, and K. E. Kim, "The hydrometeor classification algorithm for the polarimetric WSR-88D: Description and application to an MCS," *Weather Forecast.*, vol. 24, no. 3, pp. 730–748, Jun. 2009.

[13] M. A. Rico-Ramirez and I. D. Cluckie, "Classification of ground clutter and anomalous propagation using dual-polarization weather radar," *IEEE Trans. Geosci. Remote Sens.*, vol. 46, no. 7, pp. 1892–1904, Jul. 2008.

[14] V. M. Melnikov, P. Zhang, D. S. Zrnić, and A. Ryzhkov, *Recombination of super resolution data and ground clutter recognition on the polarimetric WSR-88D*, NSSL, Norman, OK. [Online]. Available: http://publications.nssl.noaa.gov/wsr88d_reports/Super_Res_and_CLutterRPT2.pdf

[15] S. M. Torres and D. S. Zrnić, "Ground clutter canceling with a regression filter," *J. Atmos. Ocean. Technol.*, vol. 16, no. 10, pp. 1364–1372, Oct. 1999.

[16] P. Clark and T. Niblett, "The CN2 induction algorithm," *Mach. Learn.*, vol. 3, no. 4, pp. 261–283, 1989.

[17] B. Cestnik, "Estimating probabilities: A crucial task in machine learning," in *Proc. 9th Eur. Conf. Artif. Intell.*, Stockholm, Sweden, 1990, pp. 147–149.

[18] P. Langley, W. Iba, and K. Thompson, "An analysis of Bayesian classifiers," in *Proc. 10th Nat. Conf. Artif. Intell.*, San Jose, CA, 1990, pp. 223–228.

[19] P. Domingos and M. Pazzani, "On the optimality of the simple Bayesian classifier under zero-one loss," *Mach. Learn.*, vol. 29, no. 2/3, pp. 103–130, 1997.

[20] M. Fang and R. J. Doviak, "Coupled contributions in the Doppler radar spectrum width equation," *J. Atmos. Ocean. Technol.*, vol. 25, no. 12, pp. 2245–2258, Dec. 2008.

[21] D. A. Holdsworth and I. M. Reid, "A simple model of atmospheric radar backscatter: Description and application to the full correlation analysis of spaced antenna data," *Radio Sci.*, vol. 30, no. 4, pp. 1263–1280, Jul./Aug. 1995.

[22] G. Zhang, L. Tsang, and Y. Kuga, "Numerical studies of the detection of targets in clutter by using angular correlation function and angular correlation imaging," *Microw. Opt. Technol. Lett.*, vol. 17, no. 2, pp. 82–86, Feb. 1998.

[23] C. Capsoni, M. D'Amico, and R. Nebuloni, "A multi parameter polarimetric radar simulator," *J. Atmos. Ocean. Technol.*, vol. 18, no. 11, pp. 1799–1809, Nov. 2001.

[24] *NEXRAD Technical Requirements*, NEXRAD Joint System Progr. Off. (SPO1), Silver Spring, MD, 1991.

[25] F. J. Harris, "On the use of windows for harmonic analysis with the discrete Fourier transform," *Proc. IEEE*, vol. 66, no. 1, pp. 51–83, Jan. 1978.

[26] C. D. Curtis, "Exploring the capabilities of the agile beam phased array weather radar," Ph.D. dissertation, Dept. Elect. Eng., Univ. Oklahoma, Norman, OK, 2009.

[27] R. J. Doviak and D. S. Zrnić, *Doppler Radar and Weather Observations*, 2nd ed. New York: Dover, 2006.

[28] D. S. Zrnić, V. M. Melnikov, and A. V. Ryzhkov, "Correlation coefficients between horizontally and vertically polarized returns from ground clutter," *J. Atmos. Ocean. Technol.*, vol. 23, no. 3, pp. 381–394, Mar. 2006.

[29] J. Vivekanandan, D. S. Zrnić, S. M. Ellis, R. Oye, A. V. Ryzhkov, and J. Straka, "Cloud microphysics retrieval using S-band dual-polarization radar measurements," *Bull. Amer. Meteorol. Soc.*, vol. 80, no. 3, pp. 381–388, Mar. 1999.

[30] J. O. Smith, III, *Mathematics of the Discrete Fourier Transform (DFT): With Audio Applications*, 2nd ed. Menlo Park, CA: W3K, 2007.

[31] M. Fang, R. J. Doviak, and V. Melnikov, "Spectrum width measured by WSR-88D: Error sources and statistics of various weather phenomena," *J. Atmos. Ocean. Technol.*, vol. 21, no. 6, pp. 888–904, Jun. 2004.

[32] V. M. Melnikov and R. J. Doviak, "Spectrum widths from echo power differences reveal meteorological features," *J. Atmos. Ocean. Technol.*, vol. 19, no. 11, pp. 1793–1810, Nov. 2002.

[33] A. Papoulis, *Probability, Random Variables, and Stochastic Processes*. New York: McGraw-Hill, 1991.

[34] J. Han, M. Kamber, and J. Pei, *Data Mining Concepts and Techniques*, 3rd ed. San Mateo, CA: MK, 2011.

Yinguang Li received the B.S. degree in electrical engineering from Wuhan University, Wuhan, China, in 2006, and the M.S. degree in electrical and computer engineering from the University of Oklahoma, Norman, in 2009, where he is currently working toward the Ph.D. degree in electrical and computer engineering.

He is also a member of the Advanced Radar Research Center of the University of Oklahoma. His research interests include weather radar signal processing, target detection and estimation, data quality control, and weather radar polarimetry.

Guifu Zhang (S'97–M'98–SM'02) received the B.S. degrees in physics from Anhui University, Hefei, China, in 1982, the M.S. degree in radio physics from Wuhan University, Wuhan, China, in 1985, and the Ph.D. degree in electrical engineering from the University of Washington, Seattle, in 1998.

From 1985 to 1993, he was an Assistant and Associate Professor in the Department of Space Physics, Wuhan University. In 1989, he worked as a Visiting Scholar at the Communication Research Laboratory in Japan. From 1993 to 1998, he studied and worked in the Department of Electrical Engineering at the University of Washington, where he first was a Visiting Scientist and later a Ph.D. student. He was a Scientist with the National Center for Atmospheric Research during the period of 1998–2005. After that, he joined the School of Meteorology, University of Oklahoma. He formulated theory of weather radar interferometry and that of phased array radar polarimetry. His research interests include wave propagation and scattering in random and complex media, remote sensing theory and technology for geophysical applications, algorithms for retrieving physical states and processes, cloud and precipitation microphysics and model parameterization, target detection and classification, clutter identification and filtering, radar signal processing, and optimal estimation. Currently, he is interested in the design and development of polarimetric phased array radars for multimissions.

Richard J. Doviak (S'56–M'57–SM'72–F'90–LF'97) received the B.S.E.E. degree from Rensselaer Polytechnic Institute, Troy, NY, in 1956, and the M.Sc. and Ph.D. degrees from the University of Pennsylvania, Philadelphia, in 1959 and 1963, respectively.

Currently, he is a Senior Engineer with the National Severe Storms Laboratory, National Oceanic and Atmospheric Administration, Norman, OK, and an Adjunct Professor with the Department of Electrical Engineering and Department of Meteorology, University of Oklahoma, Norman. He has given short courses on radar meteorology at the U.S. National Radar Conferences (April 2006) and at American Meteorological Society (AMS) Annual meetings. He is a coauthor of the text *Doppler Radar and Weather Observations*.

Dr. Doviak is a Fellow of the AMS and the Cooperative Institute of Mesoscale Meteorological Studies of the University of Oklahoma. He was a Guest Editor for a special issue of the IEEE TRANSACTIONS ON GEOSCIENCE AND REMOTE SENSING (TGARS), an Associate Editor for the *Journal of Atmospheric and Oceanic Technology* and *the Journal of Applied Meteorology*, and an Editor of TGARS. He received the IEEE's Harry Diamond Memorial Award in 1988 for outstanding technical contributions in the field of government services in any country.

Lei Lei received the B.S. degree in electrical engineering from Wuhan University, Wuhan, China, in 2006, and the M.S. degree in electrical and computer engineering from the University of Oklahoma, Norman, in 2009, where she is currently working toward the Ph.D. degree in electrical and computer engineering, as a full time student.

She is a member of Advanced Radar Research Center, University of Oklahoma. Her research interests include weather radar signal processing, weather radar polarimetry, and antenna design.

Qing Cao (M'07) received the B.S. and M.S. degrees in electrical engineering from Wuhan University, Wuhan, China, in 1997 and 2005, respectively, and the Ph.D. degree in electrical engineering from the University of Oklahoma (OU), Norman, in 2009.

He was a Telecom Engineer in China from 1997 to 2002, working on wireless communication systems. From 2002 to 2005, he was with the Radio Wave Propagation Laboratory, Wuhan University, performing research on high-frequency ground wave radar systems. Since 2006, he has been with the Advanced Radar Research Center, OU, where he was first a Graduate Assistant, then a Postdoctoral Researcher, and currently a Research Associate. His research interests include satellite remote sensing, radar signal processing, cloud and precipitation microphysics, and radar polarimetry for precipitation estimation and forecast.

Dr. Cao has been a member of the American Meteorological Society since 2007.